PHYSICAL REVIEW B
CONDENSED MATTER

THIRD SERIES, VOLUME 51, NUMBER 21 1 JUNE 1995-I

Crystalline-amorphous transition in silicate perovskites

Mahin Hemmati
Department of Chemistry, Arizona State University, Tempe, Arizona 85287-1604

Andrew Chizmeshya
Department of Chemistry, Arizona State University, Tempe, Arizona 85287-1604
and Idaho National Engineering Laboratory, EG&G Idaho, P.O. Box 1625, Idaho Falls, Idaho 83415-2208

George H. Wolf, Peter H. Poole, Jun Shao, and C. Austen Angell
Department of Chemistry, Arizona State University, Tempe, Arizona 85287-1604
(Received 23 September 1994)

$CaSiO_3$ and $MgSiO_3$ perovskites are known to undergo solid-state crystal to amorphous transitions near ambient pressure when decompressed from their high-pressure stability fields. In order to elucidate the mechanistic aspects of this transition we have performed detailed molecular-dynamics simulations and lattice-dynamical calculations on model silicate perovskite systems using empirical rigid-ion pair potentials. In the simulations at low temperatures, the model perovskite systems transform under tension to a low-density glass composed of corner shared chains of tetrahedral silicon. The amorphization is initiated by a thermally activated step involving a soft polar optic mode in the perovskite phase at the Brillouin zone center. Progression of the system along this reaction coordinate triggers, in succession, multiple barrierless modes of instability ultimately producing a catastrophic decohesion of the lattice. An important intermediary along the reaction path is a crystalline phase where silicon is in a five-coordinate site and the alkaline-earth metal atom is in eightfold coordination. At the onset pressure, this transitory phase is itself dynamically unstable to a number of additional vibrational modes, the most relevant being those which result in transformation to a variety of tetrahedral chain silicate motifs. These results support the conjecture that stress-induced amorphization arises from the near simultaneous accessibility of multiple modes of instability in the highly metastable parent crystalline phase.

INTRODUCTION

The pressure-induced crystal-to-amorphous transition has now been documented in a number of materials.[1–15] There is growing evidence that this transition is precipitated by the arrival of one or more underlying intrinsic instabilities in the highly metastable parent crystal phase. Molecular-dynamic simulations on both ice and quartz reveal the near coincidence of the violation of one of the Born mechanical stability criteria with the onset of their pressure-induced crystal-to-amorphous transitions.[16–19] Although previous mechanistic studies have focused on the amorphization of relatively open-structured phases under compression, Jeanloz[20] and others[21,22] have pointed out that a similar phenomenon can occur for dense high-pressure crystalline phases on their decompression route. In fact, a much earlier report of a solid-state crystalline-amorphous transition was that of the high-pressure stishovite phase of SiO_2, where silicon is in octahedral coordination. Although this high-pressure crystalline phase can be recovered at ambient pressure, it gradually inverts to a tetrahedral-framework silica glass when heated to only 300 °C.[23,24]

Similar behavior has also been observed for the silicate perovskites. Liu and Ringwood[25] found that $CaSiO_3$, which crystallizes in the dense cubic perovskite structure above 15 GPa, undergoes a solid-state crystal-to-amorphous transition on decompression. Although successful attempts have been recently made to preserve the metastable $CaSiO_3$ perovskite phase down to ambient pressure, this phase completely amorphizes within hours or days, even at room temperature.[26] A ^{29}Si NMR study of $CaSiO_3$ samples recovered from the perovskite stability field reveal that silicon in the amorphous phase predominantly exists in tetrahedral sites with a small fraction occupying a five-coordinate site.[26]

$MgSiO_3$ crystallizes in an orthorhombic (*Pbnm*) perovskite structure above about 23 GPa.[27,28] This

perovskite phase is retained on decompression to ambient pressure. However, on heating to only modest temperatures (as low as 150°C), the crystalline $MgSiO_3$ perovskite gradually transforms to a low-density amorphous phase with silicon in tetrahedral coordination.[29]

These observations suggest that the decompression amorphization of dense high-pressure silicate phases may be precipitated by an intrinsic instability in the SiO_6 octahedron ultimately resulting in an octahedral to tetrahedral silicon coordination change. There is some suggestion that five-coordinate silicon may be an important species along this reversion route.[26] Of further interest is the possibility that crystalline phases containing five-coordinate silicon could be accessible via metastable routes and may perhaps exhibit novel material properties.

With these ideas in mind, we have undertaken a broad investigation of the metastable reversion of alkaline earth silicate perovskites using both molecular-dynamics simulations and lattice-dynamical calculations. From the molecular-dynamics simulations the metastability limits of the model silicate perovskite systems can be determined. Apart from any shortcomings in the model potentials, the molecular-dynamic limits will always be broader than that those established on experimental time scales. From the lattice-dynamical calculations, we show that the crystal-to-amorphous transition in the silicate perovskites is initiated by a thermally activated step involving a soft polar optic mode at the Brillouin-zone center. This same mode is associated with the classic paraelectric-ferroelectric phase transformation exhibited by barium titanate perovskite. Evolution of the system along this reaction coordinate triggers, in succession, multiple barrierless modes of instability ultimately producing a catastrophic decohesion of the lattice. An important intermediary along the reaction path is a crystalline phase where silicon is in fivefold coordination and the alkaline-earth metal atoms are in eightfold-coordinated sites. At the onset pressure, this transitory phase is itself dynamically unstable to a number of additional vibrational modes. The most relevant being a dispersionless branch which condenses chains of silica tetrahedra into a variety of pyroxene-related motifs. Our results on these model silicate perovskite systems, support the conjecture that stress-induced amorphization of crystals arises from the near simultaneous arrival of multiple modes of instability in the highly metastable parent crystalline phase.

CALCULATION DETAILS

In both the molecular-dynamics simulations and lattice-dynamical calculations we have employed rigid-ion pair potentials. For $MgSiO_3$ we use the potentials developed by Matsui[30] and adapt these for $CaSiO_3$ by increasing the cation size parameter (= 0.1275 nm) to obtain agreement with the room-temperature experimental equation of state of calcium silicate perovskite.[31] The static lattice (athermal) structural properties and equation of state were calculated allowing both $GdFeO_3$ (*Pbnm*) and $BaTiO_3$ (*P4mm*)-type distortions of the ideal cubic perovskite (*Pm3m*) structure. At positive pressures, $CaSiO_3$ was found to have the lowest free energy in the ideal cubic perovskite phase whereas $MgSiO_3$ was most stable in the *Pbnm* polytype. For both systems the calculations are consistent with the experimental structural data.[31–36] Generally, we find that the behavior of both $MgSiO_3$ and $CaSiO_3$ perovskite in the metastable region is very similar. Thus, for pedagogical reasons we report here only detailed dynamical calculations for the $CaSiO_3$ system; in particular, the phonon-dispersion curves of $CaSiO_3$ perovskite are much less daunting than those of $MgSiO_3$ due to its higher symmetry.

The quasiharmonic lattice-dynamical calculations of the phonon vibrational modes were made over the entire volume range studied for $CaSiO_3$ in both the cubic perovskite *Pm3m* structure and metastable *P4mm* and *P4bm* perovskitelike phases (to be described below). Vibrational modes were calculated throughout the irreducible wedges of the respective Brillouin zones. The reported elastic moduli are athermal values of the static lattice obtained from the calculated acoustic velocities in the long-wavelength limit.

The molecular dynamic (MD) simulations were made using both constant volume and constant pressure algorithms. In both algorithms, constant temperature ensembles (ranging from 50–300 K) were employed using 2 fsec time steps. Simulations were performed on systems having both cubic (625 ions) and orthorhombic (540 ions) primary cells with periodic boundary conditions. The point Coulomb contribution to the energy and forces were calculated using full Ewald summations. Thermodynamic quantities were obtained by averaging over 2000 steps after sufficient time was allowed for equilibration. The equilibration was rapid (typically <2000 steps) since no defects arose in the structure until the onset of the instability was reached.

The infrared absorption spectrum was also obtained for the molecular-dynamics runs by calculating the Fourier transform of the electrical flux autocorrelation function.[37] The peak frequencies obtained in the absorption spectrum are found to be in excellent agreement with the Brillouin-zone center values of the transverse optic modes calculated from lattice dynamics.

RESULTS AND DISCUSSION

The equations of state of $CaSiO_3$ and $MgSiO_3$ perovskite obtained from both the athermal static lattice calculations and the 300 K molecular-dynamic simulations are shown in Fig. 1. At positive pressures, the calculated 300 K isotherms are in excellent agreement with experiment. In both the $CaSiO_3$ and $MgSiO_3$ perovskite systems at 300 K, there is a sharp break in slope in the MD equation of state under tension near -18 GPa, indicating the onset of a phase transformation. This pressure corresponds to a volume of 31 cm^3/mol for $CaSiO_3$ and 27 cm^3/mol for $MgSiO_3$. We find that the critical volume at which the onset of the transition occurs is nearly independent of temperature. However, there is a significant temperature dependence to the transition pressure. With decreasing temperature the onset of the transition occurs at increasingly higher tension, such that at

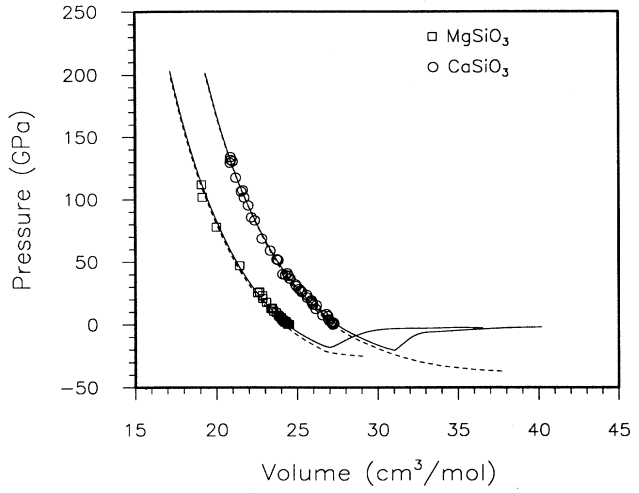

FIG. 1. Equations of state for $CaSiO_3$ and $MgSiO_3$ perovskite. Solid lines are results from the 300 K constant volume MD simulations. Dashed lines correspond to the static lattice (athermal) calculations. The experimental data for $CaSiO_3$ (Refs. 31 and 36) and $MgSiO_3$ (Refs. 34 and 35) is displayed with open symbols. The onset of amorphization are the constant volume and constant pressure MD simulations occurs at 31 cm^3/mol for $CaSiO_3$ perovskite and 27 cm^3/mol for $MgSiO_3$ perovskite, both occurring under tension near −18 GPa at 300 K. At larger volumes there is a gradual buildup of lattice defects with a reduction in tension.

50 K the onset of the transition in $CaSiO_3$ occurs at nearly −22 GPa.

It is important to point out that the onset of the phase transition in these systems occurs at nearly the same pressures regardless of whether the simulations are performed under constant volume or constant stress conditions. From this observation it can be inferred that large-scale volume fluctuations do not play a primary role in initiating the phase transition. However, within the transition region the trajectories of the simulation systems depend critically on the boundary conditions. For example, in the constant pressure simulations on $CaSiO_3$ and $MgSiO_3$ carried out under tensions exceeding −18 GPa at 300 K, there is an uncontrolled rupture or cavitation of the system. This rupture occurs because the state formed at the beginning stages of the transition cannot support such an extreme tensile stress. However, in the constant volume simulations, the system evolves in a more controlled manner. As the volume is incrementally increased within the transition region, the system reequilibrates with a reduction in the average tension of the system.

Using the constant volume simulations, it is possible to explore the structural evolution of the system throughout the transition region. We find that for $CaSiO_3$ there is a gradual loss of structural cohesion as the volume is increased beyond 31 cm^3/mol at 300 K. This disorder arises from the formation of "broken" or elongated Si-O and Ca-O bonds which results in the reduction of both the silicon and calcium average coordination numbers. With further incremental increases in volume, these defects become more numerous and the structure more disordered ultimately leading to an x-ray amorphous system by a volume of 40 cm^3/mol. The progressive loss of long-range structural cohesion is evident in the Si-O and Ca-O pair distribution functions displayed in Fig. 2. At 40 cm^3/mol, the average rms atomic displacement from the initial perovskite configuration is only 0.11 nm with all excursions less than 0.28 nm. These small excursions are consistent with a diffusionless transition, which would naturally be expected to occur in solid state amorphization at room temperature.

The average coordination number of silicon and calcium for the $CaSiO_3$ system at 300 K as a function of increasing volume is plotted in Fig. 3(a). In 3(b), the evolution of the silicon speciation distribution is displayed. The onset of the disordering at 31 cm^3/mol is marked by an onset in the reduction of both the average silicon and calcium coordination numbers. By a volume of 45 cm^3/mol essentially all of the silicon atoms are tetrahedrally coordinated and the calcium atoms are in octahedral coordination. Five-coordinated silicon occur as a transitional species between 31 and 45 cm^3/mol.

Experimentally it is found that the short-ranged structure of glasses derived from the solid-state amorphization of silicate perovskite is similar to that of normal thermal-quenched metasilicate glass.[26,29] In both glasses, silicon primarily occurs in tetrahedral coordination. At ambient pressure, the experimental volume of melt-quenched $CaSiO_3$ glass is 40.05 cm^3/mol. In MD simulations of the melt-quenched glass at this same volume (the pressure is 0.52 GPa), silicon is almost entirely in tetrahedral coordination, the average coordination number of 4.04, while the average coordination of calcium is 6.2. By comparison, in the simulated pressure-vitrified glass at this same volume (the pressure is −1.96 GPa) the average silicon coordination is 4.2, with about 15% of

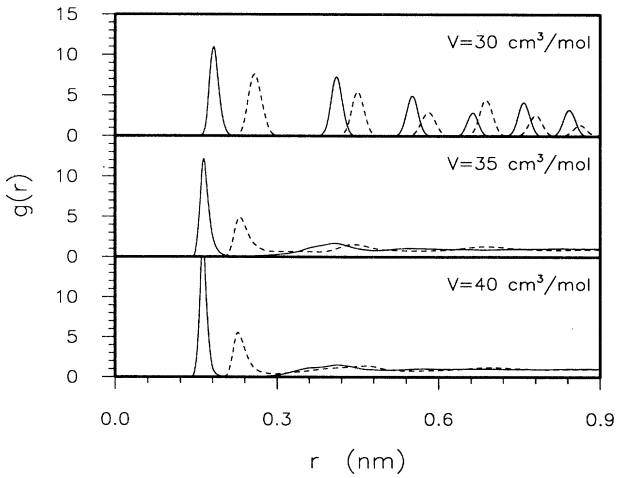

FIG. 2. Si-O (solid line) and Ca-O (dashed line) pair correlation functions for $CaSiO_3$ at 300 K and volumes for 30, 35, and 40 cm^3/mol.

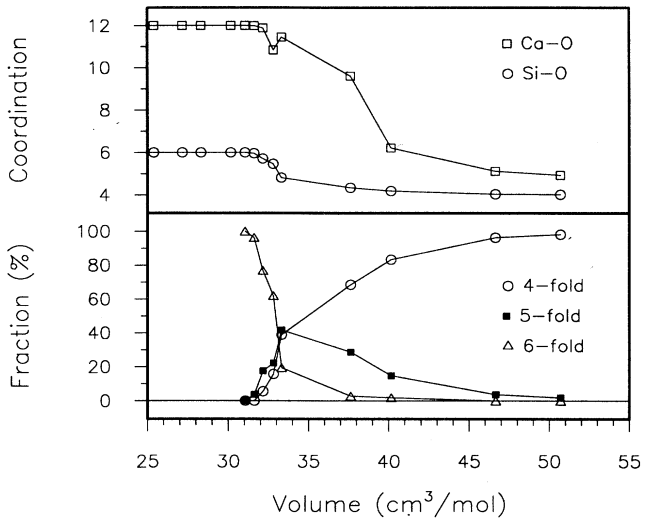

FIG. 3. (a) Volume dependence of the average silicon and calcium coordination numbers of $CaSiO_3$ obtained from the MD simulatins at 300 K. (b) Volume dependence of the silicon speciation distribution.

the silicon atoms in a five-coordinate site, while the average calcium coordination is 6.2. There is experimental evidence based on ^{29}Si NMR that the amorphous phase formed from $CaSiO_3$ perovskite on decompression does contain a resolvable fraction of the silicon atoms in a five-coordinate site.[26]

It is important to point out that the constant volume algorithms do not truly mimic the nonequilibrium experimental conditions which exist in samples undergoing a pressure-induced crystal-to-amorphous transition. In particular, the limited box sizes required in the simulations severely restrict the maximum wavelength strain fluctuations. Although this restriction appears to have little influence on the initiation of the crystal-to-amorphous transition in these systems, it does significantly influence the actual trajectories of the system within the transition region. Furthermore, the speed at which the system is pressurized through the transition region, relative to internal structural relaxation times, will also certainly influence the system's trajectory. In the constant volume molecular-dynamic simulations, we use the undistorted perovskite structure for the initial configuration of the crystal. The system is then allowed to evolve from the initial undistorted configuration to its final state with the same volume. Hence we are not able to directly address the effect of pressurization rates on the specific trajectories followed by the system. Nevertheless, even in light of these shortcomings, the constant volume simulations do provide some insights into the underlying structural features and dominant reaction pathways in the nonequilibrium region.

In support of these calculations for the $CaSiO_3$ and $MgSiO_3$ systems, we note that the structural changes found here for the constant volume simulations are quite similar to those which we have also found for a model $BaSiO_3$ perovskite system. The fundamental difference in the case of $BaSiO_3$, however, is that the analogous transition occurs in this system at positive pressures and hence, without cavitation. Here, the final amorphous product obtained from the constant pressure runs for $BaSiO_3$ perovskite is similar to that which we find from constant volume runs.

Lattice-dynamical and total-energy calculations provide more detailed information about the destabilization pathways. From a careful analysis of the critical vibrational modes in the pressure region of the crystal-to-amorphous transition, the most likely trajectories for nonequilibrium system can be inferred. First, we have made calculations of the elastic constants as a function of volume to determine whether the transition in these silicate perovskite systems can be linked to any underlying mechanical instabilities. In general, for a crystal to be stable against all infinite wavelength strain fluctuations the Born elastic stability criteria must be met. For cubic crystals the requisite criteria are that the bulk modulus, $K=(C_{11}+2C_{12})/3$, and the pure shear moduli, $G=C_{44}$ and $G'=(C_{11}-C_{12})/2$, are all positive definite.

In Fig. 4 we plot K, G, and G' as a function of volume for the cubic perovskite $CaSiO_3$ phase, calculated from the acoustic-phonon velocities of the defect-free static lattice. In $CaSiO_3$ perovskite, all of these moduli are positive at 31.0 cm^3/mol, the volume at the onset of the structural disordering observed in the constant volume and constant pressure MD simulations. With increasing volume of the static lattice, the first Born criterion to be violated is that for the pure shear moduli, G', which vanishes at a volume of about 36 cm^3/mol. This is followed by an instability in the bulk modulus K at a volume of about 41 cm^3/mol. The vanishing of G' indicates an instability in the crystal with respect to tetragonal distor-

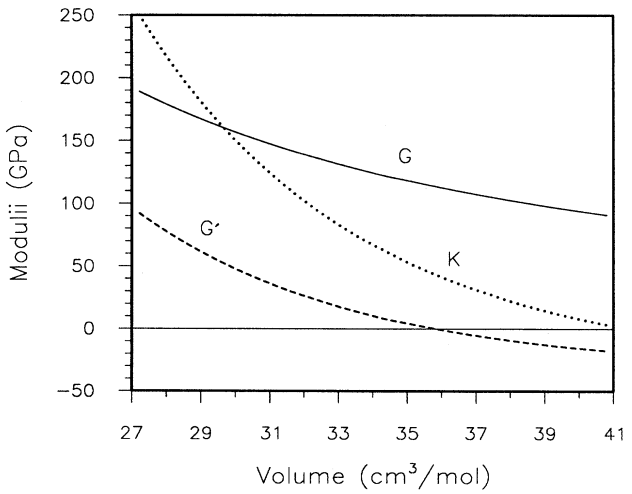

FIG. 4. Evaluation of the Born stability criteria for $CaSiO_3$ perovskite as a function of volume derived from the lattice-dynamical calculations. The first mechanical instability in the *Pm3m* structure occurs for G' at 36 cm^3/mol followed by an instability in K at 41 cm^3/mol. Note that all of the generalized moduli are positive at 31 cm^3/mol, the onset of structural disordering observed in the constant volume MD simulations.

tions of the cubic lattice whereas vanishing of K indicates an instability with respect to volume fluctuations.

Although the crystal-to-amorphous transition in these silicate perovskites does not appear to be triggered by a mechanical instability, it does appear to be triggered by a dynamical instability in a polar transverse optic mode at the Brillouin-zone center. In Fig. 5 we plot the volume dependence of the three (doubly degenerate) transverse-optic mode frequencies at the Γ point for $CaSiO_3$ perovskite in the ideal cubic structure. The mode frequencies displayed in this plot were obtained from both the quasiharmonic lattice-dynamical calculations and the molecular-dynamic simulations. In the latter, the mode frequencies correspond to maxima in the Fourier transform of the electrical flux autocorrelation function. With increasing tension, the first quasiharmonic mode frequency to vanish is that of the lowest-lying transverse-optic mode at a volume of 32.0 cm^3/mol. This volume is only slightly larger than that observed for the onset of the crystalline-amorphous transition in the 300 K MD simulations. The near coincidence of the vanishing of the transverse-optic mode frequency and the onset of disordering in the MD simulations strongly suggests that this mode plays an important role in triggering the catastrophic progression of the $CaSiO_3$ system to an amorphous state.

At the Brillouin-zone center, the transverse-optic modes all have the same symmetry (Γ_{15}) and hence can couple with each other. At the smallest volumes the highest frequency transverse-optic mode primarily arises from an antisymmetric stretch (ν_1) of the SiO_6 octahedra. The mid- and low-frequency transverse-optic modes primarily involve octahedral bending deformations with either out-of-phase or in-phase cation (Si-Ca) translations.

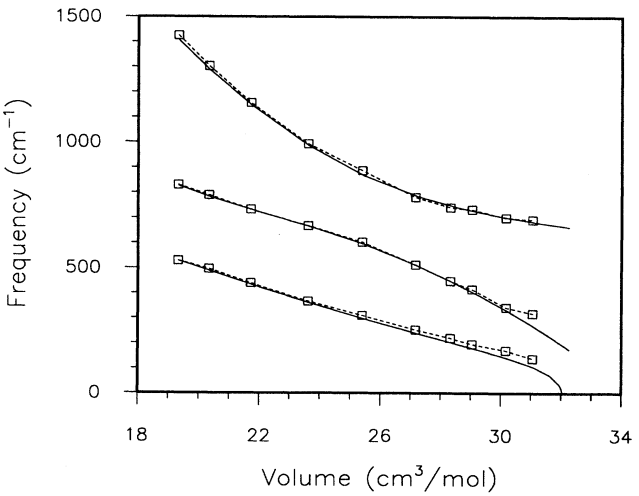

FIG. 5. Volume dependence of the transverse-optic mode frequencies (Γ_{15}) at the Brillouin-zone center of the cubic perovskite *Pm3m* phase of $CaSiO_3$. Solid lines are the quasiharmonic frequencies calculated from lattice dynamics and dashed lines with symbols are frequencies obtained from the MD simulations at 300 K through a Fourier transform of the electrical flux autocorrelation function.

Starting at the smallest volumes, the high-frequency ν_1 mode decreases the most rapidly with increasing volume. Due to a symmetry-avoided crossing at larger volumes this mode strongly couples to the two lower-frequency deformation modes. Ultimately, the lowest-frequency transverse mode condenses at a volume of 32 cm^3/mol. The atomic motions involved in this mode at the instability volume primarily involve an in-phase translation of both the silicon and calcium ions along the octahedral axial direction with an out-of-phase translation of the oxygen atoms along the same axes. This same low-frequency polar optic mode is related to the classic ferroelectric distortion exhibited by cubic $BaTiO_3$ perovskite on cooling from high temperatures. In $BaTiO_3$ perovskite, this ferroic mode couples in second order to the G' and K elastic moduli thus resulting in a tetragonal *P4mm* distortion and discontinuous volume change of the lattice at the paraelectric-ferroelectric phase transition.

To further investigate the primary reaction pathway involved in the crystalline-amorphous transition in $CaSiO_3$ perovskite we have calculated the enthalpy of the defect-free static lattice along the *Pm3m-P4mm* reaction coordinate. The relation of the *P4mm* phase to the parent *Pm3m* perovskite phase is displayed in Fig. 6(a). For this reaction coordinate there are five degrees of freedom: three internal coordinates describing the relative displacement of the Ca, Si, and O atoms in the z direction, the c/a tetragonal distortion parameter, and the lattice volume. In Fig. 6(b) we give the static lattice enthalpy as a function of c/a along the reaction coordinate for various values of the pressure. At each pressure and c/a value, the four remaining structural parameters were optimized to give the minimum enthalpy. At zero pressure the enthalpy monotonically increases with increasing distortion along the *P4mm* reaction coordinate. However, as the pressure is decreased a secondary minimum develops on the enthalpy surface. At about -12 GPa the enthalpy at this secondary minimum is equal to that of the cubic perovskite phase. In this phase the c/a ratio is roughly equal to $\sqrt{2}$ and the volume is approximately 20% larger than that of the cubic perovskite phase. At the minimum, the silicon atoms in the *P4mm* phase have moved along the octahedron axial direction of the pseudo-five-coordinated site within the square pyramid polyhedra. The calcium atoms in this phase have moved off of the perovskite mirror plane and lie in the eightfold-coordinated sites.

At -12 GPa the enthalpy barrier between these two phases is approximately 1100 K. With increasing tension the depth of the enthalpy minimum of the *P4mm* phase decreases dramatically relative to that of cubic perovskite. At -18 GPa, the pressure at which the onset of the disordering is observed in the MD simulations at 300 K, the enthalpy barrier is only about 300 K. However, at this tension, the *P4mm* phase cannot be stabilized. In fact, the *P4mm* phase itself becomes dynamically unstable at tensions in excess of about -12.5 GPa. Lattice-dynamical calculations reveal that the first vibrational mode to become unstable in the *P4mm* phase is a SiO_5 polyhedra rotational mode along the edge of the Brillouin zone between the $Z(001)$ and $A(111)$ points as

is evident in Fig. 7. This mode occurs at a **k** vector of (0.636,0.636,1) and results in a doubling of the unit cell in the *c* direction but is incommensurate with the underlying *P4mm* lattice in the *ab* plane. The incommensuration, however, lies fairly close to that of a cell tripling point in the *a* and *b* directions.

Lattice-dynamical dispersion relations along symmetry directions for the *P4mm* phase at −12, −18, and −20 GPa are shown in Fig. 7. At −18 GPa, the pressure of the onset of the initial thermally activated step, there are a number of unstable phonon branches which occur in the *P4mm* structure. The most dominant of these is a transverse-acoustic branch which is unstable throughout

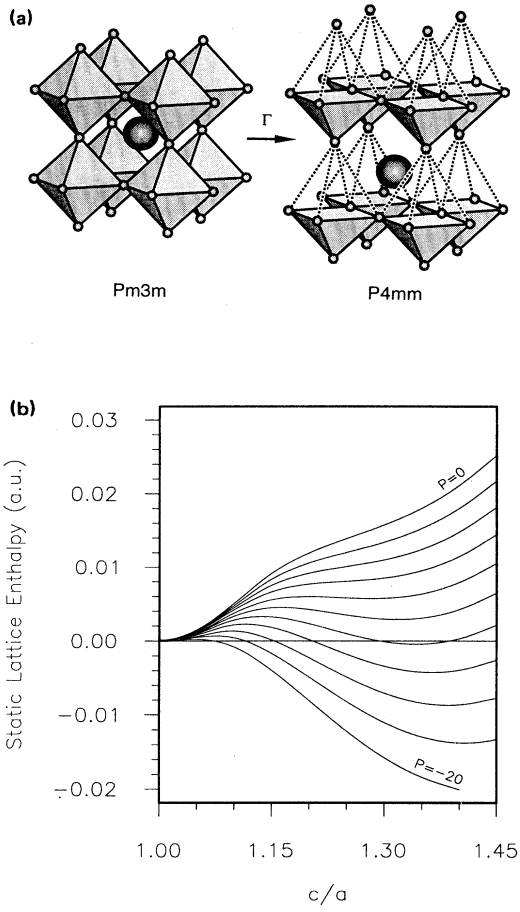

FIG. 6. (a) Structural change along the *Pm3m*→*P4mm* reaction coordinate. (b) Constant pressure enthalpy surfaces for the $CaSiO_3$ perovskite static lattice as a function of the *c*/*a* ratio along the *Pm3m*→*P4mm* reaction coordinate (the constant *P* surfaces range from 0 to −20 GPa in 2 GPa increments). With increasing tension a minimum develops in the enthalpy surface near *a*/*c* value equal to $\sqrt{2}$. At this minimum, silicon is in fivefold coordination and calcium is in octahedral coordination. The *Pm3m* and *P4mm* phases have the same enthalpy at about −12 GPa and are both mechanically and dynamically stable at this pressure.

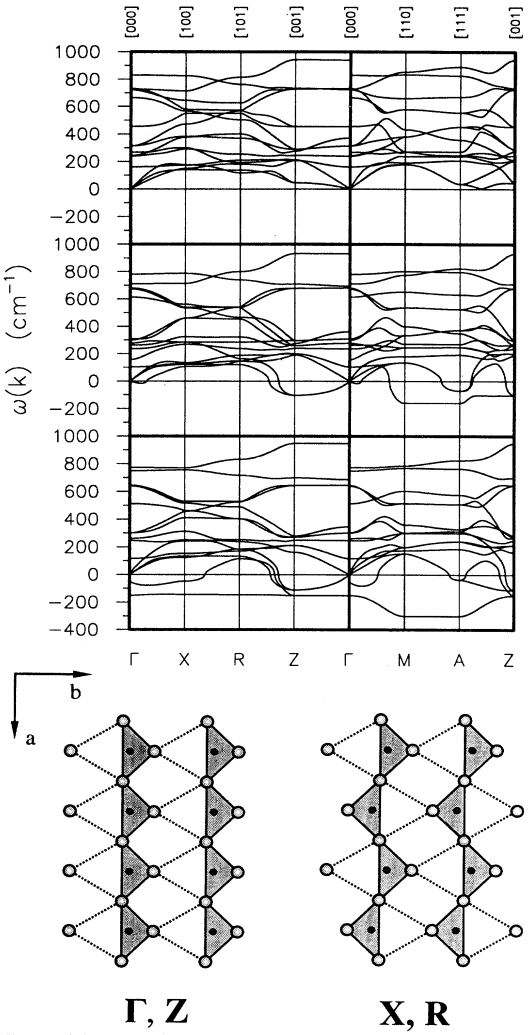

FIG. 7. (a) Quasiharmonic phonon-dispersion relations for the $CaSiO_3$ *P4mm* phase at −12, −18, and −20 GPa. At −12 GPa the *P4mm* phase is dynamically stable. The first instability occurs at −12.5 GPA for an incommensurate mode along the Brillouin-zone boundary between *A* and *Z* at **k**=(0.636, 0.636,1). At −18 GPa, entire acoustic branch in the Γ-*M*-*A*-*Z*-Γ plane is unstable. This branch corresponds to various rotational and deformational motions of the SiO_5 polyhedra. At −20 GPa, an entire optic branch in the Γ-*X*-*R*-*Z*-Γ plane also becomes unstable in the constrained *P4mm* structure. Condensation of any mode along this nearly dispersionless results in the transformation of the *P4mm* structure to a pyroxenelike structure made up of corner-linked chains of silica tetrahedra. (b) The different pyroxenelike structures which result from condensation of the unstable optic mode at the Γ, *Z*, *X*, and *R* points. Condensation of the Γ mode results in the formation of parallel chains of corner-shared SiO_4 tetrahedra where each tetrahedra has the same spatial orientation. Condensation at the *Z* point results in a structure similar to that obtained from Γ except that adjacent chains above and below the *a*-*b* plane (not shown in the figure) have an opposite orientation. Condensation of the *X* mode results in the formation of tetrahedral chains with a two-unit repeat in the *x* direction. Condensation at *R* results in a similar structure to that obtianed from *X* except that the orientation of the tetrahedra is opposite in adjacent chains above and below (not shown) the *a*-*b* plane.

the entire Γ-*M*-*A*-*Z*-Γ Brillouin-zone plane. This branch corresponds to various rotational and deformational motions of the SiO_5 polyhedra.

At a slightly larger tension of -20 GPa, a dispersionless low-lying optic mode in the Γ-*X*-*R*-*Z*-Γ plane also becomes unstable in the constrained *P4mm* structure. It is the modes along this infrared-active optic branch that are related to the fivefold to fourfold silicon coordination change. Condensation of any mode along this optic branch within the Γ-*X*-*R*-*Z*-Γ plane results in the transformation of the *P4mm* structure to a pyroxenelike structure made up of corner-linked chains of silica tetrahedra. In these modes, the silicon atoms within each pyramidal polyhedra displace toward one of four neighboring symmetry-related tetrahedral sites. The different pyroxene-type structures which result from the condensation of this soft optic mode at the Γ, *X*, *R*, and *Z* points are displayed in Fig. 7. The principal difference between these modes is the phase relationship of the silicon displacements in neighboring pyramidal units. For the optic mode at Γ, the silicon atoms all move toward the same tetrahedral site. Condensation of this mode results in the formation of parallel chains of corner-shared SiO_4 tetrahedra where each tetrahedron has the same spatial orientation. Due to symmetry, these chains can form along either the *x* or *y* axes. Condensation of the unstable mode at the *Z* point results in a *c*-doubled structure where the tetrahedra all have the same orientation in the *x*-*y* plane, as at the Γ point, but adjacent chains above and below have an opposite orientation. For an *X* point condensation, the tetrahedron orientation alternates along the chain direction and all adjacent chains are identical. The *R* point mode is similar to the *X* point except that the tetrahedra in adjacent chains above and below the *x*-*y* plane have an opposite orientation. Again, for all of these modes, the tetrahedral chains can form along either the *x* or *y* axes.

As mentioned, the soft optic branch related to the formation of silica tetrahedral chains does not condense in the constrained *P4mm* static structure until a tension of -20 GPa is reached. We find, however, that if the pyramidal rotational and deformational type modes which are soft in the *P4mm* structure at tensions greater than -12.5 GPa are allowed to condense and further lower the symmetry, then the optic branch related to the silicon fivefold to fourfold coordination change becomes destabilized at a much lower tension. In particular, with only the slightest deformation of the pyramidal units, this entire optic branch is unstable at -18 GPa, the pressure at the onset of the first thermally activated step which initiates the crystal-to-amorphous transition in these model silicate perovskites.

In conclusion, we can speculate on several details of the crystal-to-amorphous transition in silicate perovskites which may also have general relevance to other systems. In calcium silicate perovskite the crystal-to-amorphous transition is triggered by a soft ferroic mode whose atomic displacements lead to an intermediate crystalline phase with calcium in eightfold coordination and silicon in a pseudo-five-coordinate site. This first stage of the crystalline-to-amorphous transition is a thermally activated process which at 300 K and picosecond time scales occurs in our model system at a pressure of -18 GPa. At this pressure, the intermediate fivefold-coordinated silicon phase is only a transitory state; additional modes of instability are encountered along the reaction coordinate which connects the cubic perovskite phase and the *P4mm* ferroelectric phase. These additional instabilities do not require thermal activation and ultimately lead to an amorphous state where silicon is in tetrahedral coordination.

It seems likely that the condensation of any one unstable mode alone would simply result in a coherent displacement of the atoms without amorphization. However, it is the fact that a number of unstable modes are simultaneously encountered in the intermediate *P4mm* phase that ultimately results in the transformation to an incoherent amorphous phase. In the *P4mm* phase the soft optic branch which precipitates the coordination change is nearly dispersionless within the entire Γ-*X*-*R*-*Z*-Γ Brillouin-zone plane and thus provides a number of alternate energetically barrierless routes for the silicon fivefold to fourfold coordination change. Condensation of a single mode of this optic branch at any of the high-symmetry points in the Brillouin-zone results in the formation of pyroxenelike structures comprised of corner-linked chains of SiO_4 tetrahedra. Condensation of modes within the plane leads to incommensurate structures. The precise pathway that any particular region within a sample actually takes is critically sensitive to the stress field and temperature of the sample. Because the soft mode associated with the silicon coordination change couples so strongly to the volume, the local stress field around a nucleation site will be drastically altered as the domain grows. As a result, neighboring regions would experience a different local stress which would invariably alter the progression of instabilities in which they encounter.

Finally, it has been suspected that similar instability features may also underlie the pressure-induced crystal-to-amorphous transition in quartz and other materials.[10,17,18,38] For example, at the pressure where disordering first begins in metastable quartz, the oxygen sublattice is very close to a bcc packing with silicon in highly strained tetrahedral sites.[17,39] Neighboring these tetrahedral sites are a number of symmetry-related octahedral sites. The translation of the silicon atoms to the octahedral sites in the strained quartz lattice can likely occur via a number of distinct vibrational modes. Again, it is the activation of multiple low barrier pathways is likely to underlie the ultimate decohesion of the metastable crystal.

It is important to end with the caveat that the results presented here are only for a model silicate system. The details of the crystalline-amorphous transition in any system will certainly be dependent on the exact description of the interatomic energy surfaces employed. In this work we have used only the simplest representation of this potential surface based on the central pair approximation. It is clear that the energy surface in silicates cannot be accurately described by such a simple model, especially in attempting to model behavior across coordina-

tion changes. The fact that the transitions we observe in simulations occurs at such extreme negative pressures, instead of near ambient pressure as is experimentally observed, is a partial reflection of the inadequacy of the interatomic potentials. In particular, it is well known that an inclusion of nonspherical charge polarization is crucial for a faithful description of the energetics along the ferroelectric reaction coordinate. Irrespective of these shortcomings, however, we believe that these simulations do illuminate the fundamental mechanistic aspects which underlie the crystal-to-amorphous transition of silicate perovskites in nature.

ACKNOWLEDGMENTS

The authors thank Mary VerHelst-Voorhees and Paul McMillan for discussions related to the crystal-to-amorphous transition and Shirley Ekbundit for a critical review of the manuscript. This work has been funded in part by NSF under the ASU Materials Research Group Grant No. DMR-9121570 and under project Grants No. CHE-9012249, EAR-9105510, and DMR-9108028. A. C. was supported through the EG&G Idaho Long-Term Research Initiative under DOE Idaho Operations Office Contract No. DE-AC07-761DO1570.

[1]S. Sugai, J. Phys. C **18**, 799 (1985).
[2]Y. Fujii, M. Kowaka, and A. Onodera, J. Phys. C **18**, 789 (1985).
[3]A. Jayaraman, D. L. Wood, and R. G. Maines, Phys. Rev. B **35**, 8316 (1987).
[4]R. J. Hemley, A. P. Jephcoat, H. K. Mao, L. C. Ming, and M. H. Manghnani, Nature (London) **334**, 52 (1988).
[5]H. Sankaran, S. K. Sikka, S. M. Sharma, and R. Chidambaram, Phys. Rev. B **38**, 170 (1988).
[6]H. Sankaran, S. M. Sharma, S. K. Sikka, and R. Chidambaram, Pramana J. Phys. **35**, 177 (1990).
[7]M. B. Kruger and R. Jeanloz, Science **249**, 647 (1990).
[8]C. Meade and R. Jeanloz, Geophys. Res. Lett. **17**, 1157 (1990).
[9]Y. P. Handa, O. Mishima, and E. Whalley, J. Chem. Phys. **84**, 2766 (1986).
[10]G. H. Wolf, S. Wang, C. A. Herbst, D. J. Durben, W. F. Oliver, Z. C. Kang, and K. Halvorson, in *High-Pressure Research: Application to Earth and Planetary Sciences,* edited by Y. Syono and M. H. Manghnani (Terra Scientific, Tokyo; Am. Geophysical Union, Washington, D.C., 1992), p. 503.
[11]G. C. Serghiou and W. S. Hammack, J. Chem. Phys. **95**, 5212 (1991).
[12]G. C. Serghiou, R. R. Winters, and W. S. Hammack, Phys. Rev. Lett. **68**, 3311 (1992).
[13]G. C. Serghiou and W. S. Hammack, J. Chem. Phys. **98**, 9830 (1993).
[14]J. H. Nguyen, M. B. Kruger, and R. Jeanloz, Phys. Rev. B **49**, 3734 (1994).
[15]J. S. Tse, D. D. Klug, J. A. Ripmeester, S. Desgrenlers, and K. Lagarec, Nature (London) **369**, 724 (1994).
[16]J. S. Tse, J. Chem. Phys. **96**, 5482 (1992).
[17]N. Binggeli and J. R. Chelikowsky, Phys. Rev. Lett. **69**, 2220 (1992).
[18]S. L. Chaplot and S. K. Sikka, Phys. Rev. B **47**, 5710 (1993).
[19]N. Binggeli, N. R. Keskar, and J. R. Chelikowsky, Phys. Rev. B **49**, 3075 (1994).
[20]R. Jeanloz, Eos. **65**, 1245 (1984).
[21]P. Richet, Nature (London) **331**, 56 (1988).
[22]D. D. Klug, Y. P. Handa, and J. S. Tse, J. Chem. Phys. **90**, 2390 (1989).
[23]B. J. Skinner and J. J. Fahey, J. Geophys. Res. **68**, 5595 (1963).
[24]P. Gillet, A. Le Cleac'h, and M. Madon, J. Geophys. Res. **95**, 21 635 (1990).
[25]L.-G. Liu and A. E. Ringwood, Earth Planet. Sci. Lett. **28**, 209 (1975).
[26]M. Kanzaki, J. F. Stebbins, and X. Xue, Geophys. Res. Lett. **18**, 463 (1991).
[27]L.-G. Liu, Geophys. Res. Lett. **1**, 277 (1974).
[28]L.-G. Liu, Geophys. Res. Lett. **2**, 417 (1975).
[29]D. J. Durben and G. H. Wolf, Am. Mineral. **77**, 890 (1992).
[30]M. Matsui, Phys. Chem. Min. **16**, 234 (1988).
[31]M. Tarrida and P. Richet, Geophys. Res. Lett. **16**, 1351 (1989).
[32]T. Yagi, H. K. Mao, and P. M. Bell, in *Advances in Physical Geochemistry,* edited by S. K. Saxena (Springer-Verlag, New York, 1979), Vol. 2, p. 317.
[33]H. Horiuchi, E. Ito, and D. J. Weidner, Am. Mineral. **72**, 357 (1987).
[34]E. Knittle and R. Jeanloz, Science **235**, 668 (1987).
[35]H. K. Mao, R. J. Hemley, J. F. Shu, L. C. Chen, A. P. Jephcoat, Y. Wu, and W. A. Bassett, J. Geophys. Res. **96**, 8069 (1991).
[36]H. K. Mao, L. C. Chen, R. J. Hemley, A. P. Jephcoat, Y. Wu, and W. A. Bassett, J. Geophys. Res. **94**, 17 889 (1989).
[37]B. Boulard, J. Keiffer, C. C. Phifer, and C. A. Angell, J. Non-Cryst. Solids **140**, 350 (1992).
[38]J. Wang, S. Yip, S. R. Phillpot, and D. Wolf, Phys. Rev. Lett. **71**, 4182 (1993).
[39]H. Sowa, Z. Kristallogr. **184**, 257 (1988).